

Supplemental Information for:

**Amyloid assembly is dominated by mis-registered kinetic traps on
an unbiased energy landscape**

Zhiguang Jia¹, Jeremy D. Schmit^{3} and Jianhan Chen^{1,2*}*

¹Department of Chemistry and

²Department of Biochemistry and Molecular Biology, University of Massachusetts,

Amherst, MA 01003, USA

³ Department of Physics,

Kansas State University

Manhattan, KS 66506, USA

*Corresponding Authors: Phone: (413) 545-3386 (JC); (785) 532-1621 (JS)

Email: jianhanc@umass.edu (JC), schmit@phys.ksu.edu (JS)

SI Methods

Enumeration of peptide H-bond registries

To enumerate all possible register states, we first define the registries by the peptide orientation (antiparallel or parallel), contact surface (“even” or “odd”) and alignment (shift -2, 0 or 2) using a notation similar to our previous work(1) (Fig. 2 A and B). As illustrated in Fig. 2 B, an in-register state “antiparallel e|e|0” denotes the state where the even face of incoming peptide docks on the even face of the fibril core in antiparallel orientation with 0 shift (in-register). As the two H-bonds involving the same residue are close in space and are highly correlated in both formation and breakage transitions(1) (Fig. 2A), the transitions in the MSM model present the formation and breakage of H-bond pairs rather than individual bonds. The shift value increases or decreases by 2 between registries docked with same surfaces. Note that, although registries with up to 6/-6 are possible, the binding lifetimes scale exponentially with the number of possible H-bonds(2, 3). As such, states with two or fewer pairs of H-bonds contribute minimally to the sampling of registries. These states are thus grouped into the non-registered states and not described explicitly in the MSM model. In the current model, the hydrogen bond pair is identified by the peptide orientation and the pair of incoming/core peptide residues involved. For example, there are four possible H-bond pairs in the “antiparallel e|e|0” state (antiparallel 16-22, antiparallel 18-20, antiparallel 20-18 and antiparallel 22-16); the “antiparallel e|e|0” registry contains a series of sub-states defined by the formed hydrogen bond pair (e.g. 16-22|18-20 represent the states which the two hydrogen bond pairs on the N-terminus of incoming peptide is formed, whereas the other residues in the C-terminus are still unbound and free).

Explicit solvent sampling of transitions between H-bond states

All simulations were performed using Gromacs2016(4, 5) with the CHARMM36m all-atom force field(6, 7) and TIP3P water model(8). The MD time step was set at 2 fs. Electrostatic interactions were described by using the Particle Mesh Ewald (PME) algorithm(9) with a cutoff of 12 Å. Van der Waals interactions were cutoff at 12 Å with a smooth switching function starting at 10 Å. Covalent bonds to hydrogen atoms were constrained by the SHAKE algorithm.(10) The temperature was maintained at 298 K using the Nose-Hoover thermostat(11, 12). The pressure was maintained semi-isotropically at 1 bar using the Parrinello–Rahman barostat algorithm.(13)

In all simulations, the positions of all backbone heavy atoms in the core were harmonically restrained using a force constant of 10 kcal/mol/Å². The solvated systems were then neutralized by adding 150 mM NaCl.

It has been shown that Aβ₁₆₋₂₂ forms bilayer or multilayer β-sheets in solution.(14, 15) As such, we included two layers of anti-parallel β-sheets to represent the preformed fibril. Specifically, as illustrated in Fig. S1, each layer contains a pentamer, which corresponds to the approximate size of the critical nucleus of fibril formation.(16, 17) Each fibril has two docking sites available for incoming peptides (Fig. S1, yellow strand on each end of the fibril). Therefore, for each registry two incoming peptides were first docked on the core in fully H-bonded conformations (one on each end). Then for each hydrogen bond pair within the registry a set of 50 production simulations of 50 ns each in length were performed with a single hydrogen bond pair restrained (e.g, Fig 2C shows the restraint of bond 19-19). The aim of these simulation is sampling of H-bond transitions around the anchoring pair (e.g. breakage and formation of 17-21 and 21-17 when 19-19 is restrained). Before each simulation starts, the heavy atoms of the incoming residue involved in the H-bond pair are restrained and the system is heated at 800 K for 100 ps. During heating, the unrestrained part of incoming peptide is partially disordered (the core peptides will not be affected as they are always restrained). Thus, each simulation starts from a random state in which 1-4 H-bond pairs are formed

In the previous implicit solvent study(1), it was found that the kinetics of H-bond transitions mainly depend on the orientation of the peptide (parallel vs. antiparallel), the contacting residues, and the length of “free” peptide chains adjacent to the given H-bond pair before/after transition (free chain length, or FCL). For example, the transition “antiparallel 2 0 LYS:GLU” describes the formation of an antiparallel hydrogen bond pair of the terminal residues. The formation of H-bonds between LYS and GLU on the incoming and core peptides, respectively, results in a reduction in the FCL from two to zero. The implication is that the peptide reconfiguration time is fast in implicit solvent and H-bond transition kinetics are independent of the dissociated peptide conformational state. However, this is no longer true when explicit solvent is included in simulation. Aβ₁₆₋₂₂ is short and intrinsically disordered; we observed that the formation kinetics of a given H-bond pair, as noted above, also depends on the secondary structure state of the incoming peptide. Furthermore, analysis of the transition times shows that only two states,

“extended” and “coil”, need to be considered. For a particular residue on the incoming peptide, the state is defined by the secondary structure of the preceding and/or subsequent residues (if available). For example, for residue 17, the secondary structure of 16-18 is first determined by their phi/psi angle (Fig S7). If residues 16-18 all adopt β structure, the residue 17 is considered to be in the “extended” states. If any of these residues does not adopt β structure, then residue 17 is assigned to the “coiled” state. As such, two sets of formation kinetic parameters will be collected for each H-bond pair, depending on whether the residue of the incoming peptide is in “extended” or “coil” state. Accordingly, the corresponding H-bond sub-states from our previous MSM model are split into two states, depending on the secondary structure state of the incoming peptide (see Fig. 2C).

Registered states are defined using both H-bonding and backbone torsion angles

We focus on the fibril growth of the central hydrophobic core of A β (A β ₁₆₋₂₂, K₁₆LVFFAE₂₂), which is among the shortest sequences that form amyloid fibrils similar to those by full-length A β .(40-42) In our previous work (29), all possible H-bonded states were enumerated and MD simulations in a simple solvent accessible surface area (SASA)-based implicit solvent model (43) were performed to derive the average transition times between neighboring states. The fibril growth of the wild-type and mutant peptides (single mutation CHA19/CHA20 and double mutation CHA19CHA20) were predicted by the MSMs. However, due to the smoother energy surface of the SASA implicit solvent model and lack of solvent friction, fluctuations among non-registered states as well as structural reconfiguration of the peptide were found to be much faster than the sampling of registered states, allowing a single non-registered state to be used in the MSM. Furthermore, simple implicit solvent models like SASA are not capable of accurately describing the peptide conformational equilibria(44, 45). These factors likely contribute to an over-estimation of the reduction in the growth rate due to the double mutation (CHA19CHA20) compared to CHA19 and CHA20 single mutants. To overcome this, explicit solvent simulations were deployed in the current work, which enables more realistic transition rates to be computed and allows better sampling of peptide conformational fluctuations in non-registered as well as registered states. The non-registered conformations are clustered based on the peptide structure and peptide-fibril contacts. These clustered states can then be added to the MSM. In addition, we introduce a new type of transition between registered states, to account for slow peptide

conformational changes that can occur at comparable timescales to H-bond formation and breakage (detailed below). These transitions will also be necessary when extending the current framework to longer peptides.

H-bond transition rates of wild type and mutated A β ₁₆₋₂₂ peptides

We define registered states by the orientation of the incoming peptide (antiparallel or parallel), surfaces of the incoming and fibril core (odd or even), shift (the alignment of the incoming peptide relative to the template), free chain length (FCL, the number of dissociated residues of the incoming peptide starting from the N- or C-terminus), and the number of hydrogen bonds (Fig. 2 A, B). Simulations were performed to sample the transitions between these registered states as well as transitions between registered and non-registered states (Fig. 2 C and S2). The definition of states, structural models of the pre-formed fibril core, and all simulation set-ups are described in detail in the SI Methods section, Fig. S1 and Table S1. Analysis of the transition times of antiparallel registries suggests that average times of H-bond formation are highly correlated with the local secondary structure of the residue on the incoming peptide (Fig. S3). When the residue adopts extended (β -like) conformation, the formation times are relatively short (< 1 ns). In contrast, the H-bond formation times are much longer when the incoming residue is in the coil conformation (up to 8 ns). This secondary structure dependence, however, is distinct from the FCL dependence, which arises from the global movement of the peptide backbone between the bonded residue and peptide terminus. For residues in both extended and coil structures, larger FCL leads to longer H-bond formation times. The overall H-bond formation timescales from explicit solvent simulations are similar to those from implicit solvent simulations.⁽²⁹⁾ The H-bond breakage times, in contrast, are ~ 5 times slower in explicit solvent. In addition, the breakage rates show a weaker dependence on FCL and local secondary structure (Fig. S3C and Fig. S4) and appear to be mainly governed by peptide orientation (antiparallel or parallel) and the residue sidechains. Thus, breakage transitions involving different conformations are combined, to reduce the number of states required and improve the convergence of derived kinetic rates. Following H-bond breakage, the conformation of the newly free residue (extended/coil) is determined from restrained atomistic simulations, in which the probability of adopting the extended conformation after breakage (P_{extend}) is calculated for each residue. In the MSM simulation, a random number is generated every time a hydrogen bond pair is broken, if

the number is less than the P_{extend} of this residue, the newly free residue are considered to adopt a β -like extended conformation.

Simulations and cluster analysis of non-registered states

To simulate the transitions involving non-registered states, two sets of unrestrained simulations were performed. The first set of simulations focused on the transition between non-registered states and registered states. These simulations were started using the same structure as the restrained simulations described above, but with only the backbone heavy atoms of the fibril core harmonically restrained. The incoming peptides were unrestrained and could freely sample various bound and unbound states (Fig. S2, Table S1). The second set of simulations are performed to examine the diffusion-collision rates of the incoming peptides with the fibril core. These simulations focus on sampling the transitions between non-registered states, the separation distance b , and the escape distance q . Peptides were initially placed in a random position 28 \AA from the core layer (centers of mass separation). This distance is chosen as it is close to half of the end-to-end distance of amyloid 16-22 peptide in a fully extended state, plus the nonbond cutoff distance of the simulation (12 \AA in this work). This distance is sufficiently large such that the inter-molecular potential of mean force is only a function of the separation between the incoming peptide and core peptides and not their relative orientation.(18, 19) The q distance is set to $2b$ (56 \AA). A relatively large simulation box ($120 * 120 * 120 \text{ \AA}$) is used in these simulations, A total of 20 trials of 200 ns each in length were performed (see Fig S2).

Clustering analysis was applied to identify conformational sub-states involved in the nonspecific bound states. Three classes of features are chosen for clustering analysis. The first set of features, hydrogen bond states and SASA contact areas, describe the nature of contacts between incoming peptides and the fibril core. The second set of features, incoming peptide end-to-end distance and the number of residues in the extended (beta) conformation, describe the peptide internal conformation. The last set of features represent the relative positioning between incoming peptides and fibril core, including center of mass (COM) distance between the incoming peptide and the docking layer of the core, minimum distance between the incoming peptide and top layer of the core, and minimum distance between the incoming peptide and the rest of the core.

These features are normalized to have close to zero mean and unit variance using a Standard Scaler method(20, 21). Then the time-lagged independent component analysis (tICA) method is used to reduce the dimensionality.(22-24) The simulation trajectories are clustered into micro-states using a hybrid k-centers k-medoids algorithm(21). The kinetically related micro-states are lumped into macro-states using Perron Cluster Cluster Analysis (PCCAplus) algorithm(25, 26). The generalized matrix Rayleigh quotient (GMRQ) method(24, 27) is applied to optimize the hyperparameters as described in previous studies(28, 29).

Simulations of mutated peptides and model validation

The first set of simulations (the incoming peptide is restrained in all sub-states for each registry) (see Fig S2) were repeated for two mutant sequences in which phenylalanine residues at positions 19 or 19/20 are replaced with the non-natural amino acid cyclohexylalanine (CHA19 and CHA1920). For the second set of simulations (the incoming peptide is unrestrained in all sub-states of the registry), only the registries directly related to the mutation (e.g. antiparallel o|o|0 which contains three pair 17-21, 19-19 and 21-17) were repeated. To validate the MSM model, an additional set of simulations was performed for two short lifetime antiparallel registries of the wild type peptide, where 100 simulations were initiated from fully H-bonded conformations lasting 200 ns each (Fig S2). These simulations yield the lifetimes of each registry in the fully bound state and provide a direct validation of the lifetimes predicted by the MSM model.

As shown in Fig.S6, lifetimes predicted by the MSM model (black trace) accurately reproduce results derived from the simulations (solid black dot), suggesting that the MSM model faithfully recapitulates the kinetics and likely mechanism of the conformational search involved in fibril elongation. This provides a solid basis for applying the final MSM model to further investigate the origin of slow fibril growth kinetics and how it is modulated by mutations.

Markov state modeling of fibril growth

Two sets of MSM simulations were performed. In the first set of MSM simulations, the peptide was started from the *b* surface and the simulations continued until the peptide evolved to either the in-registered fully bound (antiparallel o|o|0 or antiparallel e|e|0) or dissociated states (*q* surface), From these simulations, $\tau_{residence}$ and $P_{committor}$ were derived. The second set of

simulations started from fully bound in-registered states, and continued until the dissociated state was reached. From these simulations τ_{off} is derived. Each set of simulations was performed 10000 times

(5000 for fibril cores with an even surface docking layer and 5000 for cores with an odd surface docking layer). The Gillespie algorithm(30) was employed to generate stochastic trajectories of fibril growth. For each step, two random numbers (R_1 and R_2) in the interval $[0, 1]$ are generated. Given the rates k_1, k_2, \dots, k_n for all possible transitions from the current state and the sum of these rates, k_{tot} , transition $i+1$ is selected when

$$\frac{k_i}{k_{tot}} < R_1 < \frac{k_{i+1}}{k_{tot}} \quad (2)$$

The elapsed time required before transition $i+1$ occurs is set equal to

$$t = -\frac{1}{k_{tot}} \ln(1 - R_2) \quad (3)$$

The chosen state and elapsed time are appended to the trajectory, at which point the new set of accessible states is determined and the algorithm repeats.

Table S1 Summary of atomistic production simulations

Purpose	H-bond transitions around the anchoring pair	Transition between H-bonded and non-registered states	Transition between the <i>b</i>, <i>q</i> surfaces and non-registered states	Lifetimes of fully bound registries states
Peptides	WT, CHA19, and CHA1920	WT, CHA19, and CHA1920	WT	WT
Initial structures	Singly H-bonded register states	Singly H-bonded register states	random position on <i>b</i> surface	Fully H-bonded register state
Restrains	Fibril core and the initial H-bond contact pair	Fibril core	Fibril core	Fibril core
Simulations	50 ns × 50 (runs) × 50 (register states) (for all three peptides)	WT: 50 ns × 50 (runs) × 50 (register states) CHA19: 50 ns × 50 (runs) × 30 (CHA19 perturbed register states) CHA20: 50 ns × 50 (runs) × 44 (CHA1920 perturbed register states)	200 ns × 20 (runs)	200 ns × 50 (runs) × 3 (antiparallel registries)
Box size (Å)	80 x 60 x 60	80 x 60 x 60	120 x 120 x 120	80 x 60 x 60

Table S2 Averaged residence time* of registered states in wt or mutated peptides (ns)

	wt	CHA19	CHA1920
antiparallel e e 0	83.8	66.59	36.77
antiparallel o o 0	0.45	1.86	1.6
antiparallel e e 2	2.65	0.72	0.45
antiparallel e e -2	0.41	0.56	0.62
antiparallel e o 2	1.44	0.94	1.51
antiparallel e o -2	0.07	0.42	0.49
antiparallel o e 2	1.03	3.61	1.99
antiparallel o e -2	0.29	0.88	1.23
parallel e e 0	1.68	0.96	0.98
parallel o o 0	35.72	1.73	1.89
parallel o o 2	0.44	1.77	0.73
parallel o o -2	0.96	0.21	0.33
parallel e o 2	1.79	0.56	1.05
parallel e o -2	10.22	1.15	1.2
parallel o e 2	0.42	0.57	0.75
parallel o e -2	0.35	0.57	0.64

* Note, the average residence time include sub-registered states with different FCL length, which is different from the lifetime of the states start from H-bonded antiparallel registries (Fig. 5)

Table S3 Relative free energy* of registered states in wt or mutated peptides (kcal/mol)

	wt	CHA19	CHA1920
antiparallel e e 0	-11.76	-8.51	-7.63
antiparallel o o 0	-0.72	-1.14	-0.32
antiparallel e e 2	-4.87	-1.61	-0.41
antiparallel e e -2	-1.86	-1.04	-0.63
antiparallel e o 2	-4.29	-1.94	-1.84
antiparallel e o -2	0.00	-1.02	-0.48
antiparallel o e 2	-2.21	-2.13	-0.78
antiparallel o e -2	-0.17	-0.52	-0.21
parallel e e 0	-3.35	-0.59	0.00
parallel o o 0	-11.31	-4.26	-3.64
parallel o o 2	-3.21	-2.65	-0.88
parallel o o -2	-4.32	-0.33	-0.22
parallel e o 2	-3.27	0.00	-0.10
parallel e o -2	-6.17	-0.76	-0.08
parallel o e 2	-2.22	-1.20	-0.95
parallel o e -2	-2.47	-1.05	-0.56

* with respect to the state with lowest probability.

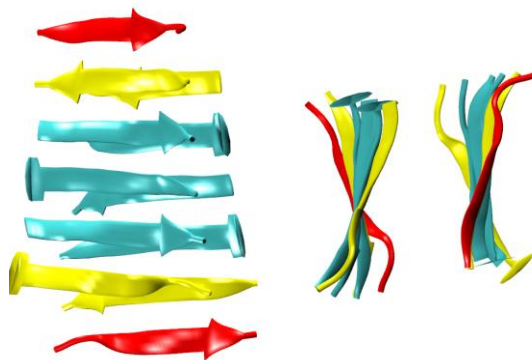


Figure S1. Side (left) and top views (right) of a representative initial structure of explicit solvent simulations (antiparallel e|e|0 registry). The peptides are shown in cartoon representations. The docking faces of the fibril core are colored in yellow and incoming peptides in purple.

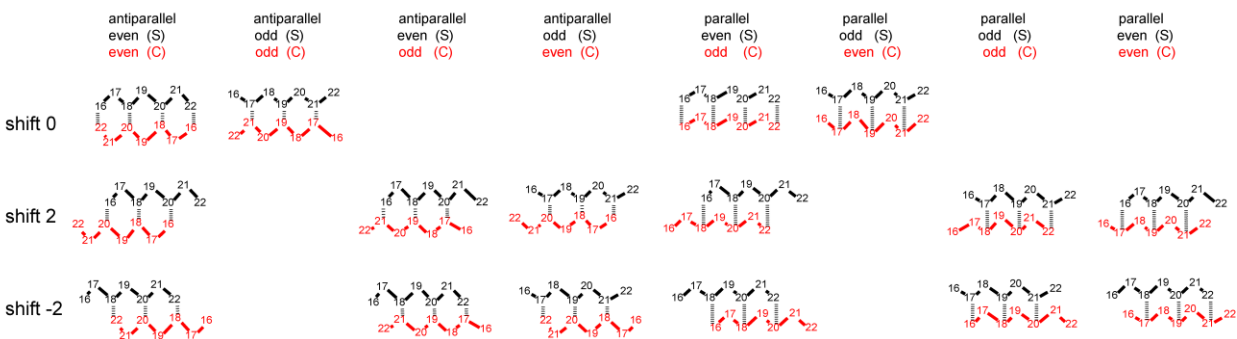


Figure S2. C) Schematic representations of all H-bond registries explicitly considered in this work (see main text). The faces (odd/even) and orientation (antiparallel/parallel) of the incoming strand (S) and core peptide (C) are given in the top row; the alignment of the incoming peptide relative to the template (shift) is listed on the left column.

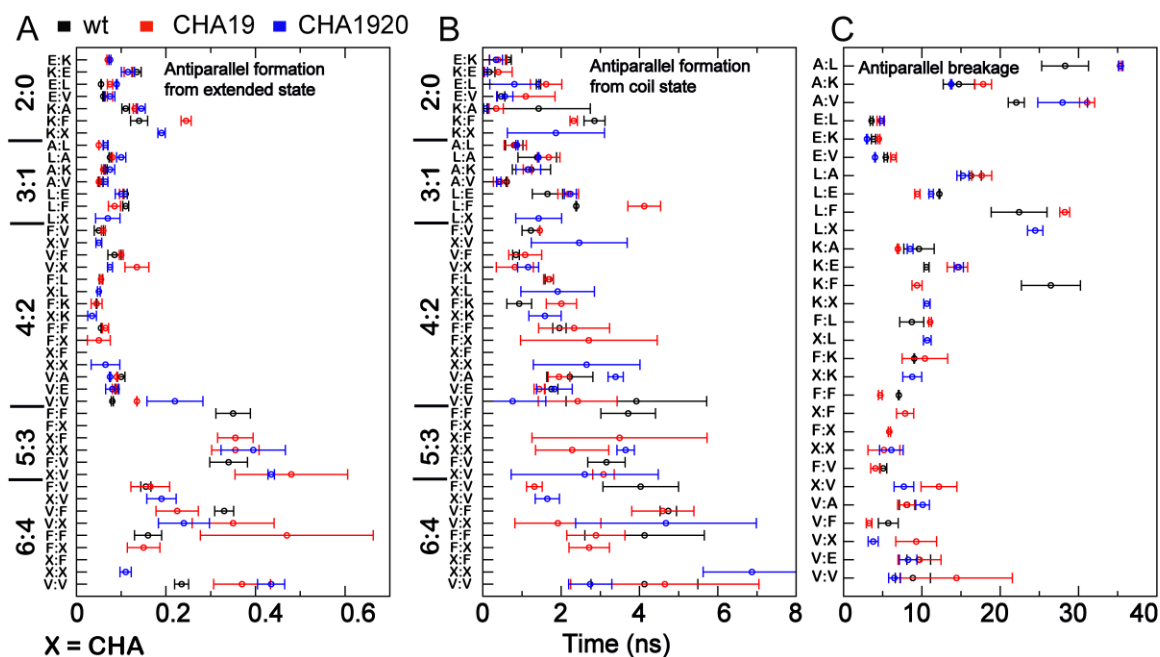


Figure S3. Average backbone H-bond pair transition times associated with anti-parallel registries: A and B) H-bond pair formation from free residue in extended and coil conformation, respectively, C) H-bond pair breakage. All transition times were derived from the restrained simulations where a selected initial H-bond contact pair was harmonically restrained. The transitions are labeled by the FCL changes (number in left) and residue pair involved in transitions. The pairs are ordered such that those with larger post-transition FCLs are at the bottom.

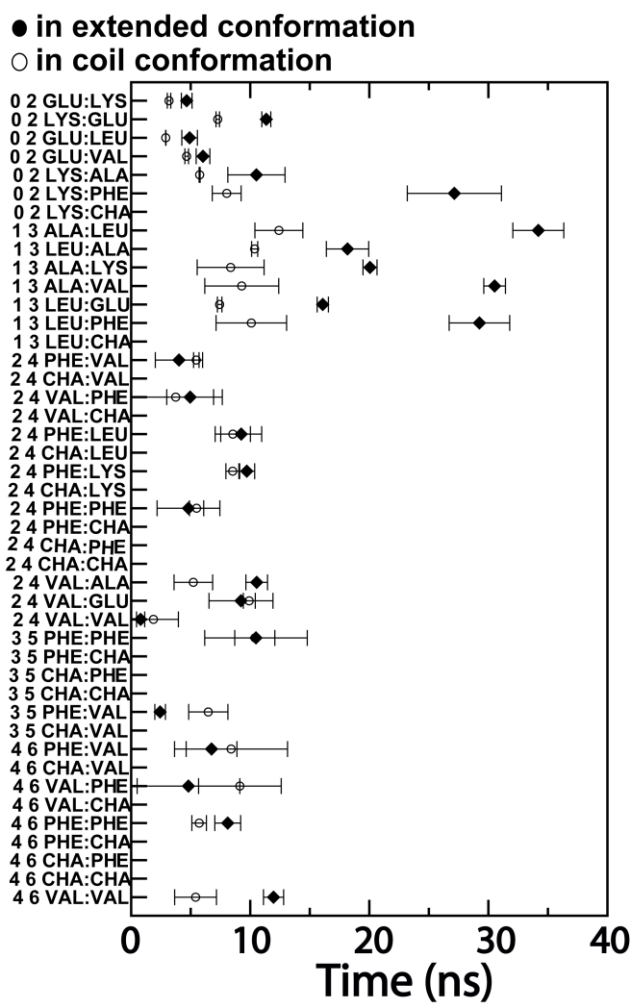


Figure S4. Average backbone H-bond pair breakage times involved different local secondary states. The solid dots represent transitions when new free residue adopt extended conformation, the open dots represent transitions when new free residue adopt coil conformation.

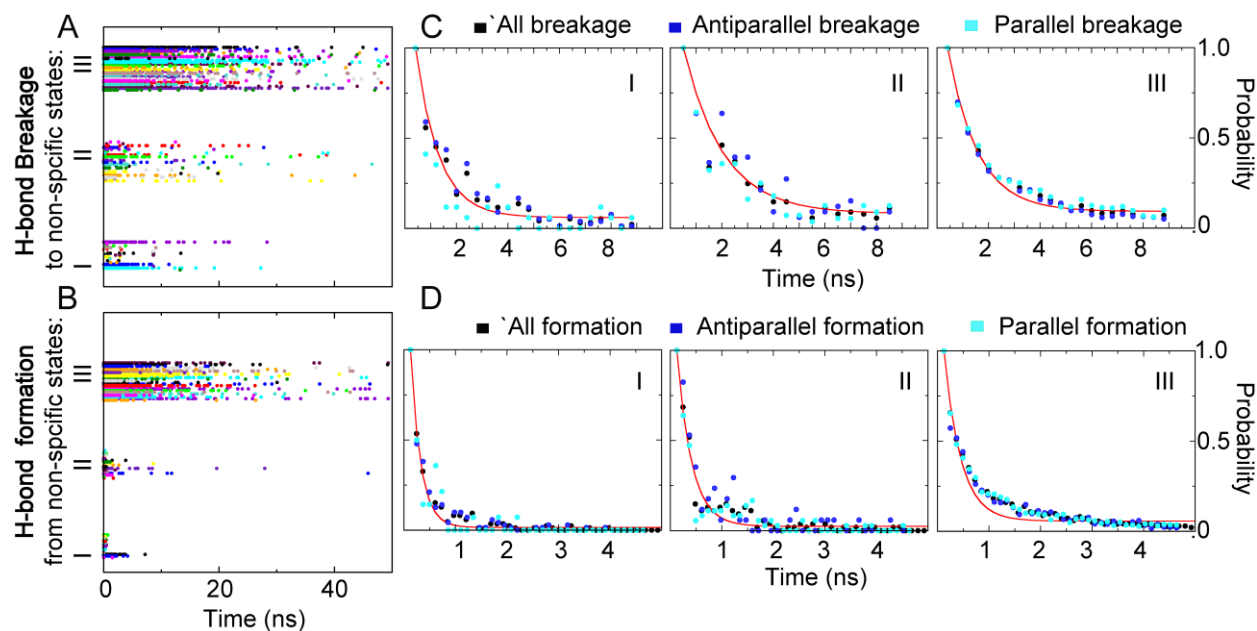


Figure S5. Transitions between registered states and non-registered states. There are three non-registered states connect to registered states, they are labelled as state I, II and III. Left panel: Transition event observed in simulations. Each individual transition event are represented as a dot in the figure. The residue pair/sidechain type are indicated by colors. Right panel: The fitted curve (red trace) use the histogram from all events (black dot). The histogram of transitions involved antiparallel orientation (blue dot) or parallel orientation (cyan dot) adopt a similar distribution around the curve.

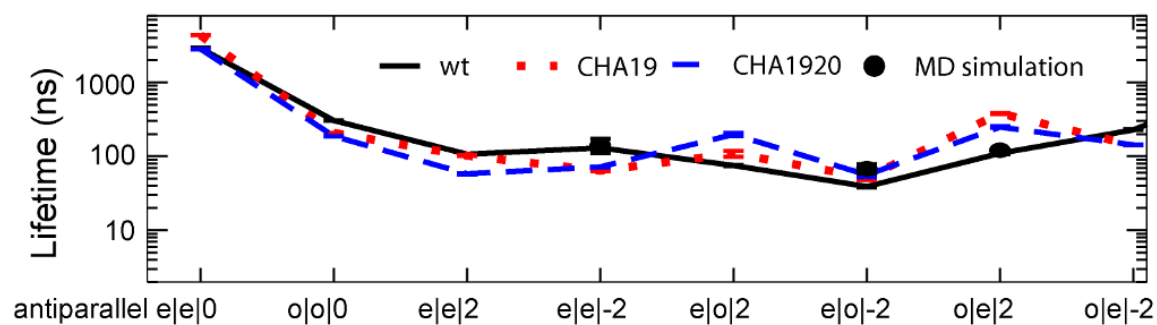


Figure S6. Average lifetimes of fully H-bonded antiparallel registries. Black solid trace and Black dot: MD vs. MSM results for antiparallel registries of the wild-type peptide. Red dot and blue dash traces: MD result of CHA19 and CHA1920 mutated peptides.

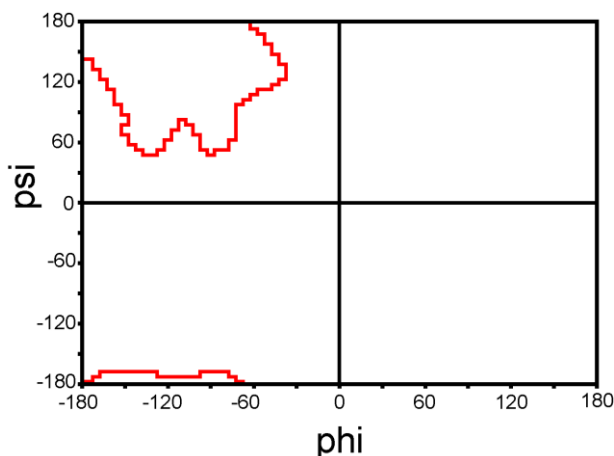


Figure S7. The Ramachandran plot of the beta region (inside red traces) in peptide secondary structure analysis.

SI References

1. Jia Z, Beugelsdijk A, Chen J, & Schmit JD (2017) The Levinthal problem in amyloid aggregation: Sampling of a flat reaction space. *The Journal of Physical Chemistry B* 121(7):1576-1586.
2. Schmit JD (2013) Kinetic theory of amyloid fibril templating. *The Journal of Chemical Physics* 138(18):185102.
3. Huang C, Ghanati E, & Schmit JD (2018) Theory of Sequence Effects in Amyloid Aggregation. *The Journal of Physical Chemistry B* 122(21):5567-5578.
4. Hess B, Kutzner C, van der Spoel D, & Lindahl E (2008) GROMACS 4: algorithms for highly efficient, load-balanced, and scalable molecular simulation. *Journal of Chemical Theory and Computation* 4(3):435-447.
5. Abraham MJ, *et al.* (2015) GROMACS: High performance molecular simulations through multi-level parallelism from laptops to supercomputers. *SoftwareX* 1–2:19-25.
6. Huang J & MacKerell AD (2013) CHARMM36 all-atom additive protein force field: Validation based on comparison to NMR data. *Journal of Computational Chemistry* 34(25):2135-2145.
7. Huang J, *et al.* (2016) CHARMM36m: an improved force field for folded and intrinsically disordered proteins. *Nature Methods* 14:71.
8. Jorgensen WL, Chandrasekhar J, Madura JD, Impey RW, & Klein ML (1983) Comparison of simple potential functions for simulating liquid water. *The Journal of Chemical Physics* 79(2):926-935.
9. Darden T, York D, & Pedersen L (1993) Particle mesh Ewald: An N -log(N) method for Ewald sums in large systems. *The Journal of Chemical Physics* 98:10089.

10. Ryckaert J-P, Ciccotti G, & Berendsen HJC (1977) Numerical integration of the cartesian equations of motion of a system with constraints: molecular dynamics of n-alkanes. *Journal of Computational Physics* 23(3):327-341.
11. Hoover WG (1985) Canonical dynamics: Equilibrium phase-space distributions. *Physical Review A* 31(3):1695-1697.
12. Nosé S (1984) A unified formulation of the constant temperature molecular dynamics methods. *The Journal of Chemical Physics* 81(1):511-519.
13. Parrinello M & Rahman A (1981) Polymorphic transitions in single crystals: A new molecular dynamics method. *Journal of Applied Physics* 52(12):7182-7190.
14. Cheon M, Chang I, & Hall Carol K (2011) Spontaneous formation of twisted A β 16-22 fibrils in large-scale molecular-dynamics simulations. *Biophysical Journal* 101(10):2493-2501.
15. Senguen FT, *et al.* (2011) Probing aromatic, hydrophobic, and steric effects on the self-assembly of an amyloid- β fragment peptide. *Molecular BioSystems* 7(2):486-496.
16. Goldsbury CS, *et al.* (2000) Studies on the in vitro assembly of A β 1–40: Implications for the search for A β fibril formation inhibitors. *Journal of Structural Biology* 130(2):217-231.
17. Hills RD & Brooks CL (2007) Hydrophobic cooperativity as a mechanism for amyloid nucleation. *J. Mol. Biol.* 368(3):894-901.
18. Northrup SH, Allison SA, & McCammon JA (1984) Brownian dynamics simulation of diffusion - influenced bimolecular reactions. *The Journal of Chemical Physics* 80(4):1517-1524.
19. Luty BA, McCammon JA, & Zhou HX (1992) Diffusive reaction rates from Brownian dynamics simulations: Replacing the outer cutoff surface by an analytical treatment. *The Journal of Chemical Physics* 97(8):5682-5686.
20. Pedregosa F, *et al.* (2011) Scikit-learn: Machine learning in Python. *Journal of machine learning research* 12(Oct):2825-2830.
21. Beauchamp KA, *et al.* (2011) MSMBuilder2: Modeling conformational dynamics on the picosecond to millisecond scale. *Journal of Chemical Theory and Computation* 7(10):3412-3419.
22. Deuffhard P, Huisinga W, Fischer A, & Schütte C (2000) Identification of almost invariant aggregates in reversible nearly uncoupled Markov chains. *Linear Algebra and its Applications* 315(1):39-59.
23. Schwantes CR & Pande VS (2013) Improvements in Markov state model construction reveal many non-native interactions in the folding of NTL9. *Journal of Chemical Theory and Computation* 9(4):2000-2009.
24. McGibbon RT & Pande VS (2015) Variational cross-validation of slow dynamical modes in molecular kinetics. *The Journal of Chemical Physics* 142(12):124105.
25. McGibbon RT, Husic BE, & Pande VS (2017) Identification of simple reaction coordinates from complex dynamics. *The Journal of Chemical Physics* 146(4):044109.
26. Deuffhard P & Weber M (2005) Robust Perron cluster analysis in conformation dynamics. *Linear Algebra and its Applications* 398:161-184.
27. Husic BE, McGibbon RT, Sultan MM, & Pande VS (2016) Optimized parameter selection reveals trends in Markov state models for protein folding. *The Journal of Chemical Physics* 145(19):194103.

28. Sultan MM, Denny RA, Unwalla R, Lovering F, & Pande VS (2017) Millisecond dynamics of BTK reveal kinome-wide conformational plasticity within the apo kinase domain. *Scientific Reports* 7(1):15604.
29. Jayachandran G, Vishal V, & Pande VS (2006) Using massively parallel simulation and Markovian models to study protein folding: Examining the dynamics of the villin headpiece. *The Journal of Chemical Physics* 124(16):164902.
30. Gillespie DT (1977) Exact stochastic simulation of coupled chemical reactions. *The Journal of Physical Chemistry* 81(25):2340-2361.